Contents lists available at SciOpen

Food Science and Human Wellness

journal homepage: https://www.sciopen.com/journal/2097-0765

China Food Publishing Co.

Mitigation of zearalenone-induced hepatocyte toxicity by peroxidase and laccase: insights from enzymatic detoxification study

Yutao Zhang[a,#], Yuting Zhang[a,#], Wei Jia[b], Xingchen Song[a], Yingjie Li[a], Yan Liu[a], Xin Liu[a], Shensheng Xiao[a], Jiangke Yang[a], Zhiyong Gong[a], Qiao Wang[a,*], Di Wu[c,*], Yongning Wu[d,*]

[a] *Key Laboratory for Deep Processing of Major Grain and Oil (Ministry of Education), College of Food Science and Engineering, Wuhan Polytechnic University, Wuhan 430023, China*
[b] *Calibra Scientific, Inc., Key Laboratory of Digital Technology in Medical Diagnostics of Zhejiang Province, Hangzhou 310024, China*
[c] *Institute for Global Food Security, School of Biological Sciences, Queen's University Belfast, Northern Ireland, Belfast BT9 5DL, UK*
[d] *NHC Key Laboratory of Food Safety Risk Assessment, China National Center for Food Safety Risk Assessment, Beijing 100021, China*

ARTICLE INFO

Article history:
Received 9 October 2024
Received in revised form 23 December 2024
Accepted 3 March 2025

Keywords:
Zearalenone
Peroxidase
Laccase
Degradation product
Hepatotoxicity evaluation

ABSTRACT

Zearalenone (ZEN), a mycotoxin present in cereals, poses significant health risks to animals and humans due to its estrogenic effects. Numerous studies on the enzymatic detoxification of ZEN have predominantly focused on reducing the parent toxin to assess the enzyme's efficacy, yet there is limited research on the identification and toxicity evaluation of the enzymatic degradation products. This study investigated the enzymatic degradation mechanisms of ZEN using commercial peroxidase (POD) and laccase (LC), with a focus on identifying degradation products and assessing their hepatotoxicity effects. Molecular docking and dynamics simulations elucidated the binding mechanisms between these enzymes and ZEN, revealing strong interactions that facilitate efficient detoxification. Subsequent analysis employing ultra-high performance liquid chromatography-high resolution mass spectrometry (UHPLC-HRMS) successfully identified crucial degradation products. Hepatic toxicity of the enzymatic degradation products was comprehensively assessed in HepaRG liver cells through systematic measurements of cell viability, oxidative stress, apoptosis, mitochondrial membrane potential, and molecular metabolic profiles. Our findings demonstrate that both POD and LC exhibit significant efficacy in mitigating hepatocyte toxicity induced by ZEN, thereby highlighting their potential utility in enhancing food safety. This research provides essential data for safety evaluation regarding enzymatic detoxification of ZEN while offering theoretical and technical resources for risk assessment related to mycotoxin enzymatic detoxification.

© 2026 Beijing Academy of Food Sciences. Publishing services by Tsinghua University Press.
This is an open access article under the CC BY-NC-ND license
(http://creativecommons.org/licenses/by-nc-nd/4.0/).

1. Introduction

Zearalenone (ZEN), a mycotoxin produced by *Fusarium* species, extensively contaminates major cereal crops worldwide, including maize, wheat, oats, and sorghum, leading to substantial economic losses annually[1]. Consumption of ZEN-contaminated feed by animals can result in the presence of ZEN and its metabolites in food products such as milk, meat, and eggs[2]. Total diet study data indicate that the average dietary exposure to ZEN among European populations ranges from 0.02 to 0.12 μg/kg body weight per day; however, high-exposure groups reach levels up to 0.25 μg/kg body weight per day, approaching the tolerable daily intake (TDI) of 0.25 μg/kg body weight per day established by the European Food Safety Authority (EFSA)[3]. Similarly, total diet studies conducted in China have reported an average dietary exposure to ZEN of 0.1 μg/kg body weight per day for adults and 0.2 μg/kg body weight per day for

# Contributed equally to this manuscript.
* Corresponding authors.
E-mail address: wangqiao8577@163.com (Q. Wang); d.wu@qub.ac.uk (D. Wu); wuyongning@cfsa.net.cn (Y.N. Wu)

Peer review under responsibility of Beijing Academy of Food Sciences.

SciOpen Publishing services by Tsinghua University Press

http://doi.org/10.26599/FSHW.2025.9250539
2213-4530/© 2026 Beijing Academy of Food Sciences. Publishing services by Tsinghua University Press. This is an open access article under the CC BY-NC-ND license (http://creativecommons.org/licenses/by-nc-nd/4.0/).

children[4]. These findings suggest that there may be a significant risk of high dietary exposure to ZEN among children which requires considerable attention. Due to its structural similarity with natural estrogens, ZEN has the ability to bind estrogen receptors and exert estrogenic effects thereby disrupting hormonal balance and causing reproductive toxicity[5]. Additionally, it exhibits immunotoxicity, hepatotoxicity, genotoxicity, teratogenicity, and carcinogenic properties[6]. Consequently, reducing contamination levels of ZEN in grains while mitigating associated health risks has become an urgent priority within global food safety.

The methods for ZEN removal from food and feed primarily encompass physical, chemical, and biological approaches[7]. In comparison to the limitations associated with chemical and physical detoxification methods, such as nutrient loss, inefficiency, and costly equipment requirements, biological strategies offer advantages of enhanced efficacy, specificity, and environmental friendliness[8]. Among these approaches, enzymatic detoxification strategies are widely acknowledged as the most preferred techniques for future practical applications. Studies investigating the degradation of ZEN and other mycotoxins have demonstrated significant potential for peroxidases (PODs) and laccases (LCs). PODs possess the ability to catalyze a wide range of oxidation reactions that enzymatically degrade various mycotoxins. Mycotoxins such as aflatoxin B_1 (AFB_1), aflatoxin M_1 (AFM_1)[9], and deoxynivalenol (DON)[10] have been reported to be degraded by PODs. Studies have indicated that PODs can significantly reduce toxin levels in food and feed matrices while exhibiting increased effectiveness under low-temperature conditions at neutral pH values[11]. LCs exhibit broad pH tolerance ranges coupled with temperature stability enabling them to maintain high activity even under diverse environmental conditions which is particularly crucial when addressing contaminants present within complex food matrices thereby allowing for broader yet more effective applications[12-13]. Numerous studies have showcased the capability of LCs derived from various sources to effectively degrade both AFB_1 and ZEN where degradation rates surpassing 90% were observed under specific conditions[14-16].

Current research on enzymatic detoxification of mycotoxins primarily focuses on reducing the parent toxins to evaluate the efficacy of enzymatic degradation[17]. However, limited studies have focused on the identification of enzymatic degradation products and their detoxification effects. In this study, we employed 2 commercial PODs and LCs to systematically investigate the impact of PODs and LCs degradation on hepatic cytotoxicity caused by ZEN, as well as to assess the toxic potency of resulting enzymatic degradation products. Through molecular docking and molecular dynamics simulations, we conducted a computational analysis of the binding affinities between ZEN and POD or LC. The initial identification of lactone ring cleavage by POD and the primary products generated by LC were examined utilizing physicochemical analytical methods. By utilizing human-derived HepaRG cell assays, we comprehensively elucidated the effects of POD and LC enzymatic degradation products on cell viability, liver function, toxic mechanisms, and metabolic levels. This systematic evaluation allowed us to assess hepatotoxicity associated with ZEN degradation products produced by POD and LC. Our study provides foundational data along with an evaluation strategy for safety assessment in relation to enzymatic detoxification of ZEN.

2. Materials and methods

2.1 Chemicals and enzymes

ZEN (purity ≥ 99%) was obtained from Shanghai Anpu Laboratory. POD (≥ 250 U/mg) from horseradish and LC (≥ 0.5 U/mg) from *Trametes versicolor* were purchased from Sigma-Aldrich, St. Louis, MO, USA. RPMI-1640 medium, 0.25% EDTA-trypsin, and dual antibiotics (penicillin and streptomycin) were acquired from Gibco, UK. Fetal bovine serum (FBS) was sourced from Biological Industries, Israel. Phosphate-buffered saline (PBS), hydrogen peroxide solution, 2,2′-azino-bis-(3-ethylbenzothiazoline-6-sulfonic acid) (ABTS), and sodium citrate buffer were acquired from Shanghai Macklin Biochemical. All experimental solutions were prepared using sterile water. The chemicals and reagents used, including formic acid, dimethyl sulfoxide (DMSO), acetonitrile, and methanol of chromatography grade, were sourced from Merck Life Science, Shanghai, China.

2.2 ZEN degradation by POD and LC

The protocols for ZEN degradation by POD and LC were adapted from previously reported methods[18-19]. Initially, 1 mL of a 30 μg/mL ZEN standard solution was evaporated under nitrogen. Subsequently, 1 mL of a mixture comprising 800 μL PBS (pH 7.0, 10 mmol/L), 100 μL H_2O_2 (100 mmol/L), and 100 μL POD (15 U/mL) was added. The sample underwent incubation at 30 °C and 150 r/min for a duration of 24 h. Following incubation, 2 mL of chloroform was introduced, the mixture was vortexed for 1 min until separation occurred, and the chloroform layer was then collected. This extraction procedure was replicated three times. The extract, after drying under nitrogen, was re-dissolved in 1 mL acetonitrile, vortexed for 30 s, and subsequently centrifuged at 12 000 r/min for 10 min. The solution was then passed through a 0.22 μm organic filter membrane for subsequent applications, yielding samples of the ZEN-POD degradation product. In a similar fashion, 1 mL of a 30 μg/mL ZEN standard solution was evaporated under nitrogen and subsequently combined with 1 mL of a solution containing 800 μL sodium citrate buffer (pH 6.0, 100 mmol/L), 100 μL ABTS (5 mmol/L), and 100 μL LC (10 U/mL). The protocols for incubation, extraction, and sample preparation were identical to those of the ZEN-POD degradation, resulting in ZEN-LC degradation product samples. Degradation of ZEN facilitated by POD and LC achieved degradation rates of (86.53 ± 3.72)% and (90.67 ± 2.87)%, respectively.

2.3 Culture and treatment of HepaRG cells

HepaRG cells, sourced from the China Center for Type Culture Collection (CCTCC), were consistently cultured in RPMI 1640 medium, supplemented with 1% penicillin/streptomycin and 10% FBS. HepaRG cells in the logarithmic growth phase were treated with 0.25% trypsin-EDTA to achieve a single-cell suspension, subsequently diluted to the desired cell density, and seeded into 96-well plates. Incubation followed at 37 °C and 5% CO_2 for 12 h. Subsequently, the experimental groups were treated as follows: 1 mL of 30 μg/mL ZEN for the ZEN group, 1 mL of 30 μg/mL

ZEN POD degradation product for the ZEN-POD group, 1 mL of 30 μg/mL ZEN LC degradation product for the ZEN-LC group, and untreated cells served as the control group. The treated wells were further incubated under conditions of 37 °C and 5% CO_2 for 24 h, preparing them for various assays. Six replicates were established for each experimental group.

2.4 Molecular docking and dynamics simulation

Molecular docking analysis was performed utilizing the AutoDock 4.2.6 software suite. The 3D structure of ZEN was retrieved from the PubChem database (PubChem CID: 5281576) and stored in sdf format. The structure was imported into OpenBabel software, the MMFF94 force field was applied, and the output was saved in pdbqt format. The crystal structures of POD and LC were sourced from the PDB database (https://www.rcsb.org/) using PDB codes 1H5A and 1KYA, respectively. The molecular structures of POD and LC were imported into AutoDock Tools for preprocessing, which involved removing water molecules and separating small co-crystallized molecules, including inhibitors and ions. Charges were assigned, and each residue was hydrogenated in AutoDock Tools, followed by terminal residue repair, force field reapplication, energy minimization, residue repair, and resolution of potential atomic collisions. The structure was subsequently saved in pdbqt format. Molecular docking was conducted via AutoDock Vina, with the docking center set to the default coordinates, and the grid size defined as 60 Å × 60 Å × 60 Å, encompassing the entire protein structure. Binding energy scores were calculated according to the docking poses and interactions between the ligand and receptor molecules.

Molecular dynamics simulations were performed using the Gromacs software (version 2022.3) for analytical and research purposes. Small molecules were pre-processed using AmberTools (version 22) with the GAFF (General AMBER Force Field). Subsequently, Gaussian 16W facilitated the hydrogenation and calculation of restrained electrostatic potential (RESP), which were integrated into the system's topology file. Simulation parameters were established at a steady temperature of 300 K and a pressure of 1 bar, employing the Amber99sb-ildn force field. The solvent employed was the Tip3p (Transferable Intermolecular Potential 3 Points) water model, with an optimal quantity of Na^+ added to neutralize the system's total charge. Initially, the molecular dynamics simulation employed the steepest descent method for energy minimization, followed by 100 000 steps of NVT (canonical ensemble) equilibration and NPT (isothermal-isobaric ensemble) equilibration, each characterized by a coupling constant of 0.1 ps over 100 ps. In the final phase, a free molecular dynamics simulation was executed, encompassing 5 000 000 steps with a step size of 2 fs, culminating in a total duration of 100 ns. Post-simulation, built-in analytical tools were employed to examine trajectories, yielding calculations for root mean square deviation (RMSD), root mean square fluctuation (RMSF), radius of gyration (R_g) and hydrogen bond number of each amino acid trajectory.

2.5 UHPLC-HRMS analysis

The ultra-high performance liquid chromatography-high resolution mass spectrometry (UHPLC-HRMS) system was employed for the identification of ZEN enzymatic degradation products and the analysis of cellular metabolomics, with analytical methods adapted from previous studies[20]. The UHPLC system utilized was UltiMate™ 3000 (Thermo Fisher Scientific, MA, USA), coupled with an HSS T3 column (2.1 mm × 100 mm, 1.8 μm, Waters, MA, USA). Mobile phase A comprised formic acid (0.1%, *V*/*V*) in water, while mobile phase B consisted of formic acid in acetonitrile (0.1%, *V*/*V*). The gradient elution profile was as follows: 0.0–1.0 min at 95% A; 1.0–8.5 min, a transition from 95% A to 0% A; 8.5–11.0 min at 0% A; 11.0–11.1 min, a shift from 0% A back to 95% A; 11.1–13.0 min maintained at 95% A. During the analysis, the column was maintained at a temperature of 40 °C, with a flow rate set at 0.3 mL/min. The mass spectrometry platform utilized was the Q-Exactive Orbitrap high-resolution mass spectrometer from Thermo Fisher Scientific (USA), equipped with an electrospray ionization (ESI) source and capable of operating in both positive and negative ion modes. Ion source settings included: collision gas: nitrogen; spray voltage: –3.5 kV/3.8 kV; capillary temperature: 350 °C. Data acquisition was conducted in FullMS-ddMS^2 scanning mode, with a full scan resolution of 140 000 and a scan range of *m/z* 75–1 000. MS^2 data were collected with a resolution of 35 000, using collision energies of 20, 40, and 60 eV.

The raw data were initially processed using Xcalibur software version 4.1. ZEN enzymatic degradation products were identified utilizing Mass Frontier version 7.0. Metabolomics data were normalized based on quality control (QC) samples using Compound Discoverer version 3.1. QC samples were prepared by pooling 50 μL aliquots from each extracted sample. These QC samples were analyzed after every 6 injections to ensure system reproducibility and monitor the stability of the mass spectrometry system throughout the analytical run.

2.6 Cell viability and biochemical indicators assay

The apparent cytotoxicity of HepaRG cells was characterized by assessing cell viability and multiple hepatic function and injury biomarkers, including alanine aminotransferase (ALT), aspartate aminotransferase (AST), alkaline phosphatase (AKP), lactate dehydrogenase (LDH), glutathione (GSH), and superoxide dismutase (SOD). Cell viability was measured using a Cell Counting Kit-8 (CCK-8) assay (Dojindo Laboratories, Japan). HepaRG cells were incubated with gradient concentrations of ZEN standard solution (0, 1, 5, 10, 20, 30, 40 μg/mL), ZEN-POD, and ZEN-LC degradation product samples in 96-well plates for 24 h. Subsequently, 10 μL of CCK-8 solution was added to each well, and the plates were incubated for an additional hour in the dark. The optical density (OD) at 450 nm was measured using a microplate reader. Cell viability was calculated based on the OD values, following the method described in the literature[21]. During the experiment, an equal volume of basal medium was used as a blank control, and medium containing 1% DMSO served as the solvent control. Hepatic biochemical biomarkers in HepaRG cells were determined using commercial enzyme-linked immunosorbent assay (ELISA) kits (Nanjing Jiancheng Bioengineering Institute, China). All experiments were performed in sextuplicate.

2.7 Live/dead staining

Cells were plated at a density of 1×10^4 cells/mL in a 96-well plate and incubated for 12 h. Following this, cells were treated with ZEN, ZEN-POD, and ZEN-LC degradation products, and subsequently incubated for an additional 24 h. The Calcein-AM assay (Thermo Fisher Scientific, USA) was utilized according to the manufacturer's protocol. Fluorescence microscopy (IX53, Olympus) was employed to examine the cells. Live cells were identified by green fluorescence at an excitation wavelength of (490 ± 10) nm, whereas dead cells exhibited red fluorescence at a 545 nm excitation wavelength. Blank and solvent controls were incorporated into the experimental design, with six replicates established for each group.

2.8 Apoptosis, reactive oxygen species (ROS) and mitochondrial membrane potential (MMP) determination

Cell apoptosis was evaluated using an Annexin V-FITC/propidium iodide (PI) Apoptosis Detection Kit (Shanghai Yisheng Biotechnology, China). The collected HepaRG cells were washed twice with PBS and the supernatant was discarded. The cells were resuspended in 100 μL of 1× Binding Buffer, followed by the addition of 5 μL Annexin V-FITC and 10 μL PI staining solution. The mixture was incubated for 10 min at room temperature in the dark. Subsequently, 400 μL of 1× Binding Buffer was added, and the cells were analyzed using a flow cytometer (CytoFlex, Beckman Coulter, USA). FITC fluorescence was detected at an excitation wavelength of 488 nm and an emission wavelength of 525 nm, while PI fluorescence was detected at an excitation wavelength of 535 nm and an emission wavelength of 615 nm. Intracellular ROS levels were measured using a DCFH-DA Fluorescent Probe Assay Kit (Shanghai Beyotime Biotechnology, China). After collection, cells were washed twice with PBS and resuspended. DCFH-DA staining solution was added to achieve a final concentration of 10 μmol/L, and the cells were incubated at 37 °C for 20 min in the dark. Subsequently, the cells were washed three times with PBS to remove excess DCFH-DA and resuspended in PBS. Flow cytometric analysis was performed using an excitation wavelength of 480 nm and an emission wavelength of 525 nm. MMP was assessed using a JC-1 MMP Assay Kit (Shanghai Yisheng Biotechnology, China). Following collection and centrifugation, cells were resuspended in 1 mL of JC-1 working solution and incubated at 37 °C for 20 min in the dark. Flow cytometric analysis was performed with excitation/emission wavelengths of 514 nm/529 nm for FITC and 585 nm/590 nm for PE. Blank controls were included in all experiments. For ROS detection, negative control (DCFH-DA probe alone) and positive control (Rosup treatment) groups were also set up. All groups were tested in 6 replicates.

2.9 Metabolism analysis

For metabolomic analysis, cells at a density of 1×10^7 cells/mL were routinely cultured and then exposed to ZEN, its POD-mediated degradation product (ZEN-POD), and its LC-mediated degradation product (ZEN-LC). Following treatment, the culture medium was discarded, and the cells were washed with PBS and collected into 15 mL centrifuge tubes. The cells were centrifuged at 1 000 r/min for 5 min at 4 °C. Subsequently, the cells were washed twice with pre-chilled PBS. After centrifugation, the supernatant was discarded, and the cell pellets were transferred to 2 mL EP tubes. The cell pellets were quenched in liquid nitrogen for 20 min. After thawing on ice, 1 mL of ice-cold methanol was added to each tube. The samples were vortexed and then centrifuged at 12 000 r/min for 10 min at 4 °C. After centrifugation, the supernatant was collected. The collected supernatant was concentrated under a nitrogen stream and reconstituted in 1 mL of the initial mobile phase. After filtration through a 0.22 μm membrane filter, the samples were subjected to UHPLC-HRMS analysis.

Raw data were initially processed using Xcalibur software (version 4.1) and normalized based on QC samples with Compound Discoverer (version 3.1). QC samples were prepared by pooling 50 μL aliquots from each extracted sample and analyzed after every 6 injections to ensure system reproducibility and monitor mass spectrometry stability throughout the analytical run. Metabolites were identified and confirmed using online databases, including mzCloud (http://www.mzcloud.org) and the Human Metabolome Database (HMDB; https://www.hmdb.ca). Metabolite data underwent dimensionality reduction and normalization using SIMCA software (version 14.0). Principal component analysis (PCA) and partial least squares discriminant analysis (PLS-DA) were performed with SIMCA-P software (version 14.1; Umetrics, Sweden). Pathway analysis was conducted using MetaboAnalyst 6.0 (http://www.metaboanalyst.ca).

2.10 Statistical analysis

All experimental data were analyzed and visualized using GraphPad Prism software version 9.5. One-way analysis of variance (ANOVA) and *P*-value calculations were performed using SPSS Statistics version 19. All results are expressed as mean ± standard deviation (SD). Fluorescence images of live/dead cells were processed using ImageJ software. Raw flow cytometry data were analyzed with FlowJo software. Metabolic pathways were visualized using the online platform Bioinformatics (https://www.bioinformatics.com.cn).

3. Results and discussion

3.1 Molecular docking and dynamics simulation analysis of ZEN with POD and LC

Initially, the potential substrate binding sites and capabilities of POD and LC with ZEN were analyzed through molecular docking. The binding model between ZEN and POD, as shown in Fig. 1A, indicates that hydrogen bonds, pi-pi conjugations, and pi-alkyl interactions are primarily responsible for their interaction. Docking results reveal that ALA-34 carbonyl of POD forms a hydrogen bond with hydroxyl hydrogen on ZEN's phenyl ring at a distance of 2.9 Å. HIS-170's ring structure forms a pi-pi conjugation with ZEN's aromatic ring at a distance of 4.3 Å while also forming a pi-alkyl interaction with ZEN's lactone ring at 4.0 Å away from each other. PHE-41 engages in two pi-alkyl interactions with the methyl on ZEN's lactone ring at distances of 4.9 Å and 4.1 Å respectively; meanwhile, HIS-42 and ARG-38 engage in pi-alkyl interactions with the methyl and aromatic rings on ZEN's lactone ring at distances of

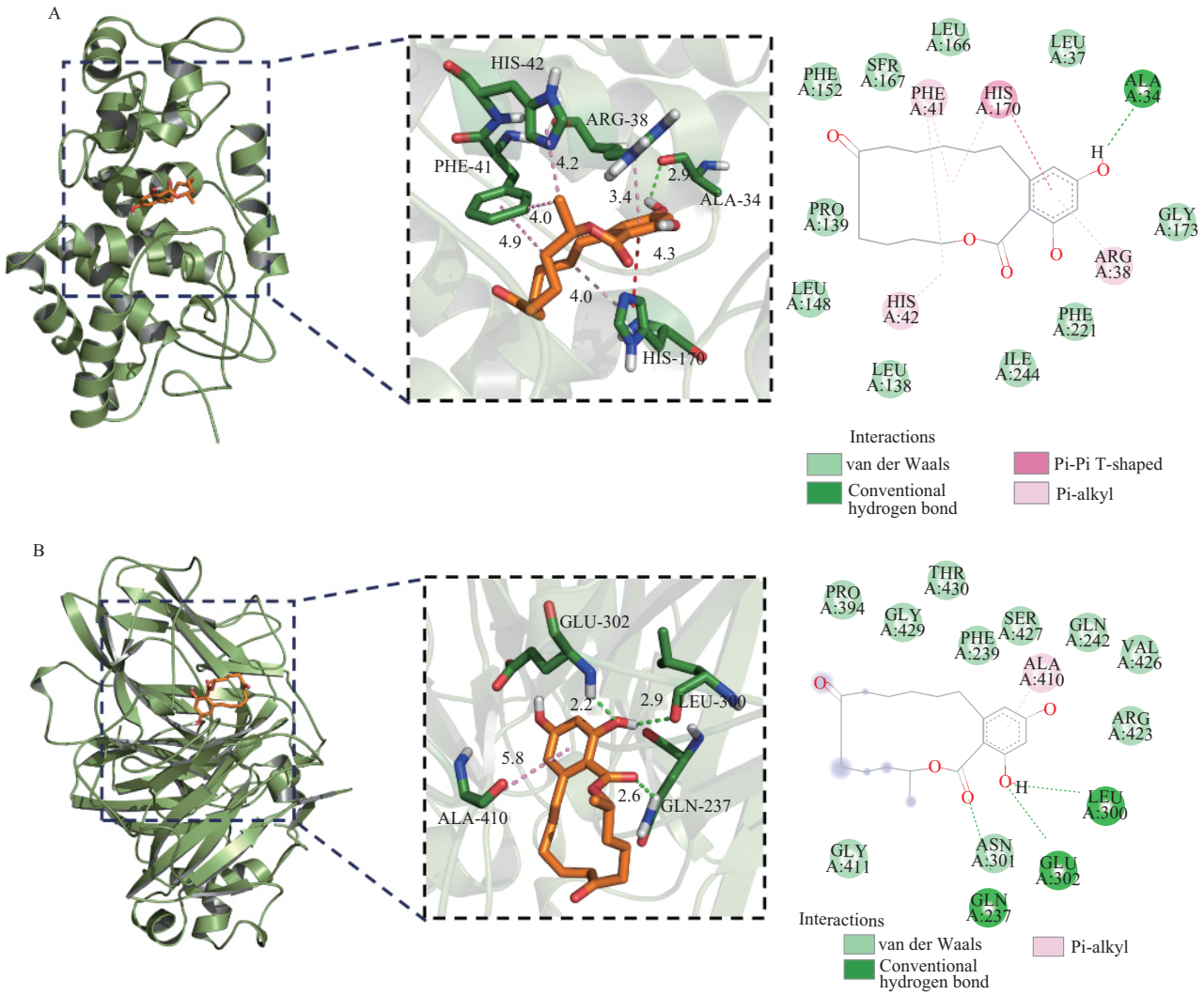


Fig. 1 Molecular docking analysis of the binding of ZEN with degrading enzymes. (A) The interaction model of ZEN with POD; (B) The interaction model of ZEN with LC.

4.2 Å and 3.4 Å respectively. The binding free energy between POD and ZEN is –8.5 kcal/mol, indicating strong affinity between them. Likewise, the binding model between LC and ZEN (Fig. 1B) involves three hydrogen bonds: GLN-237's hydroxyl hydrogen of LC forms a hydrogen bond with the carbonyl on ZEN's lactone ring at 2.6 Å, LEU-300's carbonyl interacts with the hydroxyl hydrogen on ZEN's aromatic ring at 2.9 Å, and GLU-302's amino hydrogen bonds with the hydroxyl oxygen on ZEN's aromatic ring at 2.2 Å. Additionally, ALA-410's carbonyl engages in a pi-alkyl interaction with ZEN's aromatic ring. The calculated free energy was –8.4 kcal/mol which suggests strong ability to bind. ZEN-protein complex stability increases as negative values decrease. Binding energies can be classified into three levels: below –4.25 kcal/mol indicates some binding capability, below –5.0 kcal/mol indicates strong binding capability, and below –7.0 kcal/mol indicates very strong binding capability[22]. POD and LC both exhibit robust abilities to bind ZEN, suggesting efficient catalysis towards its degradation[14,23]. The similar binding free energies of the two enzymes with ZEN may be attributed to their classification as oxidases, which share inherent similarities.

Molecular dynamics methods were employed to ascertain the atomic-level alterations in ZEN's binding with POD and LC. The root mean square deviation (RMSD) of the protein and small molecule Cα backbone elucidates the positional shifts between their conformations throughout the simulation compared to the initial conformations. As illustrated in Figs. 2A and E, the average RMSD values for the ZEN-POD and ZEN-LC complexes are (0.189 ± 0.010) and (0.206 ± 0.013) nm respectively. This consistency in RMSD values indicates that the binding of POD and LC with ZEN is stable, with variations maintained within a narrow range. The root mean square fluctuation (RMSF) results indicate an increased dynamics of residues near the active sites (Figs. 2B and F), considered crucial for enhancing substrate adaptability within enzyme mechanisms[24]. R_g analysis demonstrates that the R_g values of POD and LC remain relatively unchanged during the simulation (Figs. 2C and G). Over 100 ns, the average R_g values for POD and LC are (1.945 ± 0.010) nm and (2.220 ± 0.005) nm, respectively, suggesting that the proteins' compactness and three-dimensional structures are preserved post-binding with ZEN. Furthermore, hydrogen bond analysis reveals

that an average of 4–6 hydrogen bonds are consistently maintained between POD, LC, and ZEN (Figs. 2D and H), contributing to the stabilization of the enzyme-substrate complex. The number and stability of these hydrogen bonds are critical in elucidating the catalytic mechanisms of enzymes[25].

3.2 Screen and identification of ZEN degradation products

UHPLC-HRMS analysis was conducted on the ZEN group, ZEN-POD enzymatic group, and ZEN-LC enzymatic group, with FullMS-ddMS^2 data imported into MassFrontier 7.0 software to identify significant peaks of enzymatic products. Fragmentation patterns, precise mass-to-charge ratios of fragment ions, and neutral losses were utilized to predict the potential chemical structures of ZEN enzymatic products, which were then verified against databases and existing literature (the high-resolution mass spectrometry spectra for identification provided in Supplementary Material). The study revealed that POD catalyzes the formation of 5 ZEN degradation products, namely 15-OH-ZEN, 14-OH-ZEN-quinone, 13,15-OH-ZEN, HZEN, and DHZEN (Fig. 3). POD catalyzes the hydroxylation of ZEN at the C15 position to form 15-OH-ZEN (reaction a), which is unstable and readily autoxidizes to 14-OH-ZEN-quinone (reaction b) and 13,15-OH-ZEN (reaction c), a process confirmed using the decolorizing POD (PoDyP4) from oyster mushrooms[26]. The hydroxylation capacity of POD for ZEN aligns with previous research, which identified hydroxylation as a common pathway in mycotoxin degradation[27]. Conversely, POD degrades ZEN by cleaving its lactone bond, forming the open-ring product HZEN (reaction d), which rapidly decarboxylates to DHZEN (reaction e). This finding first demonstrates POD's ring-opening ability, enhancing our understanding of its catalytic mechanisms. In contrast to POD, LC predominantly forms fewer degradation products through oxidation, specifically hydroxylating ZEN at the C_{13} position to produce 13-OH-ZEN (reaction f), which then autoxidizes to 13,15-OH-ZEN (reaction e). This observation suggests that LC's action on ZEN is more targeted towards site-specific hydroxylation rather than extensive ring-opening or substantial structural alterations[28]. The degradation products of ZEN, catalyzed by the 2 enzymes, exhibited distinct chemical properties and biological activities, offering crucial insights for the systematic evaluation of the detoxification capabilities of enzymatic products.

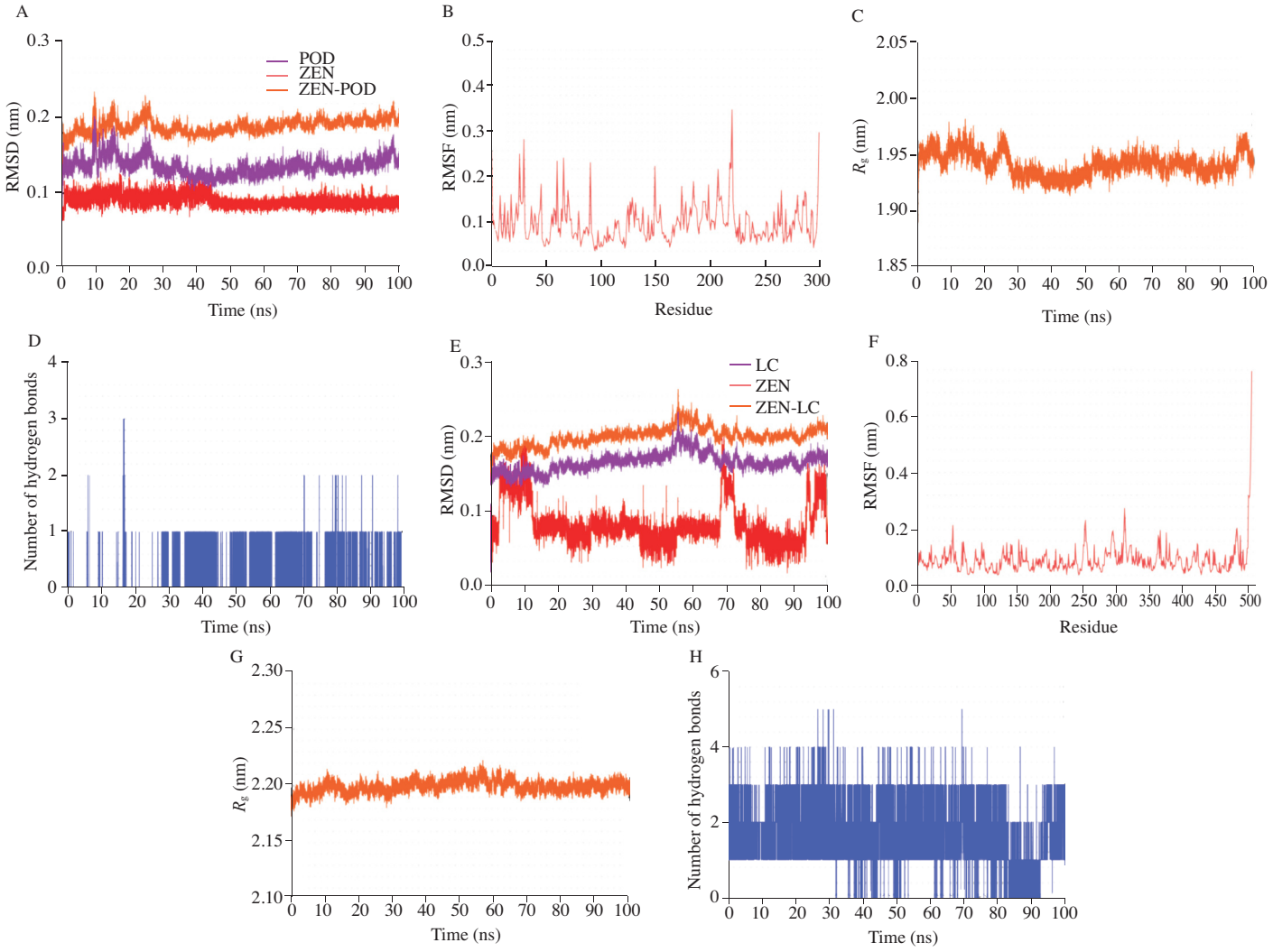


Fig. 2 Molecular dynamics simulation of ZEN and degrading enzymes. A-D correspond to the analyses of RMSD, RMSF, radius of gyration, and hydrogen bond number for ZEN and POD, respectively; E-H correspond to the analyses of RMSD, RMSF, radius of gyration, and hydrogen bond number for ZEN and LC, respectively.

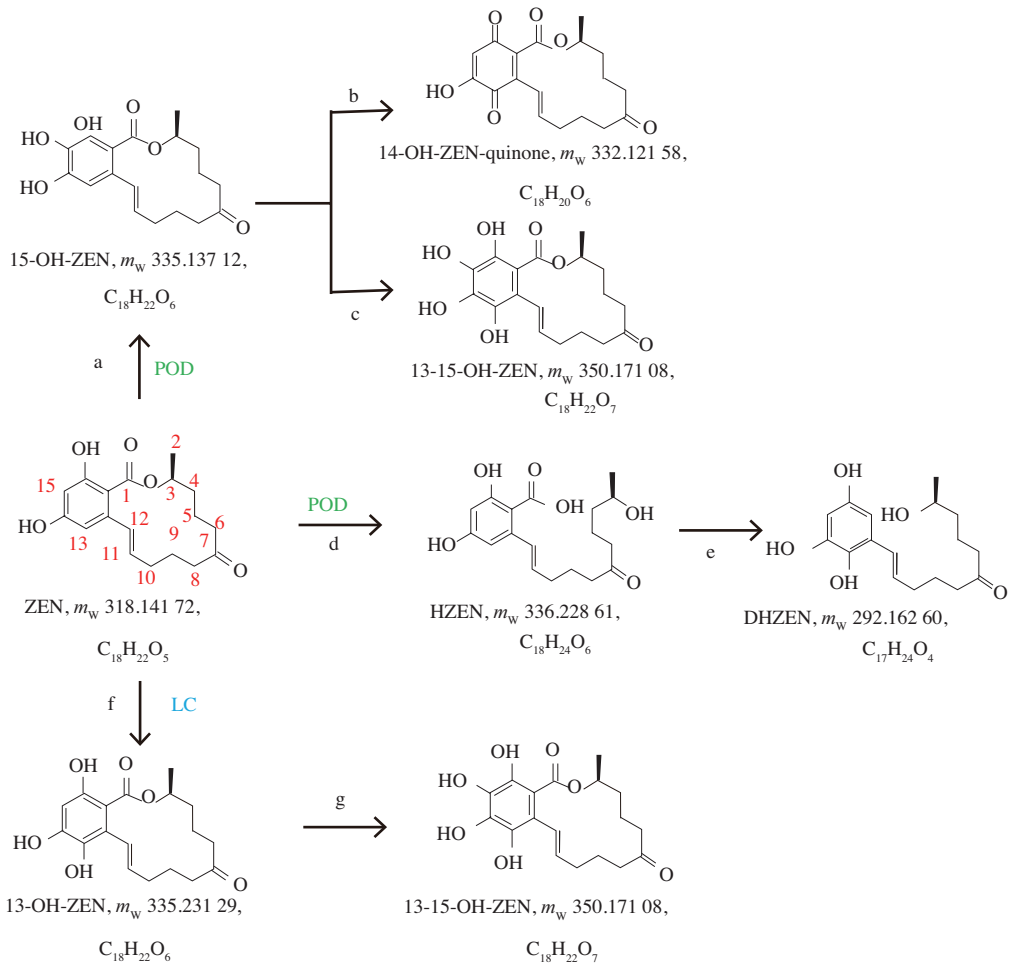


Fig. 3 Pathways of ZEN degradation mediated by POD and LC.

3.3 Cellular viability and survival state analysis

ZEN undergoes initial biotransformation in the liver within biological systems. Therefore, the human hepatocarcinoma cell line HepaRG was selected to investigate the cytotoxicity of ZEN degradation products. As shown in Fig. 4A, ZEN reduced the viability of HepaRG cells in a dose-dependent manner. Based on the observed inhibition rates at ZEN concentrations ranging from 1 to 40 μg/mL, the half-maximal inhibitory concentration (IC_{50}) of ZEN on HepaRG cells was calculated to be 31 μg/mL using GraphPad Prism software. Therefore, a concentration of 30 μg/mL was selected for subsequent cytotoxicity assays.

The effects of 30 μg/mL ZEN, ZEN-POD and ZEN-LC enzymatic degradation products at the same concentration, and the solvent control (1% DMSO) on HepaRG cell viability were assessed using the CCK-8 assay. The results indicated (Fig. 4B) that the cell viability in the solvent control group (1% DMSO) did not differ significantly from the control group, suggesting that 1% DMSO had no effect on the growth of HepaRG cells. Therefore, the use of 1% DMSO as a solvent does not interfere with the assessment of the cytotoxicity of ZEN and its enzymatic degradation products. In contrast, the ZEN-treated group exhibited a significantly lower cell viability compared to the control group ($P < 0.005$), with a survival rate of 56%, indicating that ZEN markedly inhibits the growth of HepaRG cells and possesses strong cytotoxic effects. After degradation by POD and LC, the cell survival rates increased to 91% and 87%, respectively. However, these rates still showed significant differences compared to the control and solvent groups, possibly due to incomplete degradation of ZEN by POD and LC, resulting in residual ZEN that continued to exert cytotoxic effects on the cells. Another possible reason is that the degradation products of ZEN by POD and LC still possess low-level toxicity, which may inhibit cell growth. Nevertheless, compared to the ZEN group, the cytotoxicity was significantly reduced.

Live/dead cell staining was utilized to visually compare the distribution of live and dead HepaRG cells under treatments with ZEN and its POD and LC enzymatic degradation products. After staining with Calcein-AM and PI, live cells emitted green fluorescence, while dead cells exhibited red fluorescence. As shown in Fig. 4C, observations of the control and solvent groups without staining revealed well-grown cells with intact morphology. After fluorescence staining, a large number of live cells and few dead cells were observed. In the ZEN-treated group, unstained observations showed sparsely distributed cells struggling to maintain normal morphology, with extensive cell death. The culture medium appeared red, possibly due to significant cell death leading to reduced consumption by live cells, resulting in minimal color change. After staining, a large number of dead cells were observed.

Under treatment with the POD and LC degradation products, cells observed without staining exhibited morphology nearly identical to the control group. However, post-staining, the number of dead cells was higher than in the control group but significantly lower than in the ZEN group, consistent with the cell viability results. Therefore, we preliminarily conclude that ZEN can be effectively detoxified through treatment with POD and LC.

3.4 Hepatic biochemical indices of HepaRG cell

Results from cell viability assays and live/dead cell staining indicate that the toxicity of ZEN, following enzymatic degradation by POD and LC, differs significantly from that of native ZEN. These treatments are suggested to induce alterations at the cellular physiological level. To evaluate whether hepatic injury could be induced by the POD and LC enzymatic degradation products of ZEN, we assessed the activities of ALT, AST, AKP, levels of GSH, SOD activity, and LDH in HepaRG cells. Among these biomarkers, ALT, AST, and AKP are commonly used indicators for hepatic injury assessment. The results presented in Figs. 5A-C demonstrate significant increases in ALT, AST, and AKP activities in HepaRG cells treated with ZEN alone ($P < 0.001$). In contrast, under treatment with ZEN-POD or ZEN-LC degradation products only the AST activity exhibited a significant increase within the group treated with ZEN-POD degradation product compared to control group, no significant differences were observed for AKP and ALT activities. Oxidative stress is a pivotal mechanism underlying hepatic injury[29]. The detection results for oxidative stress markers revealed a significant decrease in GSH levels (Fig. 5D) and SOD activity (Fig. 5E) in the ZEN group ($P < 0.001$), indicating the potential of ZEN to induce cellular oxidative stress. GSH plays a crucial role in converting toxic PODs into non-toxic hydroxyl compounds, thereby safeguarding membrane structure and function. SOD acts as an essential antioxidant defense mechanism by eliminating reactive free radicals during metabolic processes. Remarkably, both GSH levels and SOD activity were significantly higher in the ZEN-POD and ZEN-LC degradation product groups compared to the ZEN group ($P < 0.001$). Notably, there was no significant difference observed between the GSH levels of the ZEN-POD degradation product group and the control group. Hepatic injury is associated with nuclear translocation of LDH and pyruvate dehydrogenase complex, resulting in lactate production from nuclear pyruvate along with increased nuclear acetyl-CoA synthesis[30]. Our study demonstrated that LDH levels were significantly elevated in HepaRG cells treated with ZEN ($P < 0.001$). Conversely, LDH levels were significantly reduced in both the ZEN-POD and ZEN-LC degradation product groups compared to the ZEN group ($P < 0.001$), without any notable difference from those observed in the control group (Fig. 5F). These findings suggest that oxidative stress may contribute to hepatocellular damage induced by ZEN, while its degradation products generated by POD and LC at equivalent dosages exhibit substantially reduced toxicity compared to pure form of ZEN itself[31].

3.5 Analysis of ROS levels

ROS derived from molecular oxygen, consist of various active molecules and free radicals[32]. At moderate levels, ROS can act as second messengers in cellular signaling pathways. However,

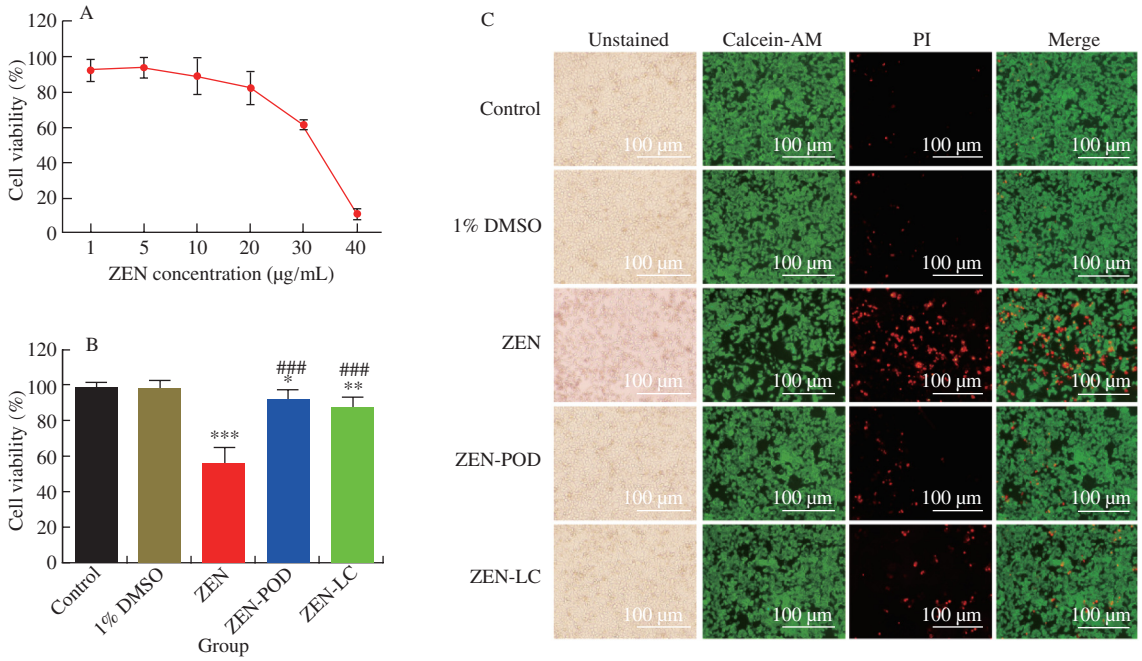


Fig. 4 Impact of ZEN, ZEN-POD and ZEN-LC enzymatic degradation products on the viability and survival status of HepaRG cells ($n = 6$). (A) Analysis of cell viability for ZEN across various concentration gradients. (B) Analysis of cell viability for ZEN, ZEN-POD and ZEN-LC enzymatic degradation products (ZEN concentration was 30 μg/mL). (C) Comparative analysis of the effects of ZEN, ZEN-POD and ZEN-LC enzymatic degradation products on live/dead cells status. * indicates statistical significance compared to the control group (* $P < 0.05$, ** $P < 0.01$, *** $P < 0.001$); # denotes statistical significance compared to the ZEN group (### $P < 0.001$). Same as below.

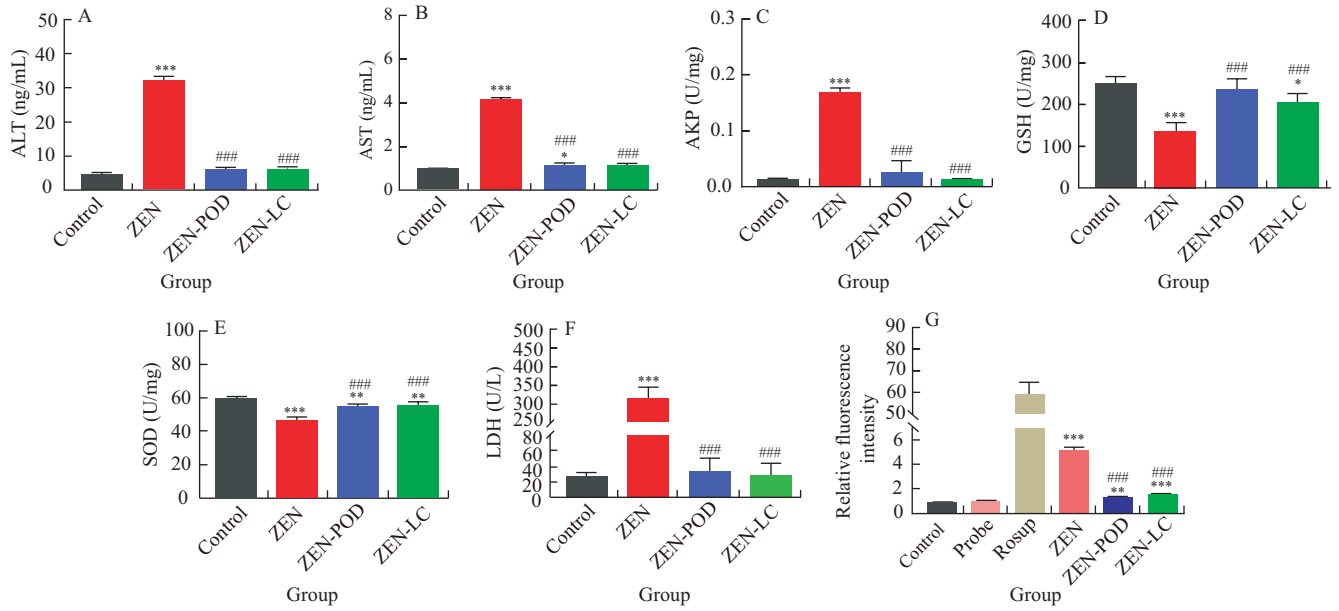


Fig. 5 Impact of ZEN, ZEN-POD and ZEN-LC enzymatic degradation products on hepatic injury markers in HepaRG cells (n = 6). A-G correspond to: ALT, AST, AKP, GSH, SOD, LDH, and ROS, respectively.

excessive ROS can lead to the onset and progression of various diseases[33]. In normal cells, the balance between ROS production and the antioxidant system is typically maintained at appropriate ROS concentrations[34]. Based on cell viability results, this study exposed HepaRG cells to 30 μg/mL ZEN and its degradation products obtained from POD and LC treatment to investigate their effects on intracellular ROS production. The levels of ROS in each group were analyzed by flow cytometry, as shown in Fig. 5G. Both the control and probe groups exhibited low levels of ROS, with fluorescence intensities of 1.13 and 1.24, respectively. In the positive control group, cells treated with the ROS inducer Rosup showed a significant increase in ROS (approximately 58.96 times compared to the control). Although the fluorescence intensity in the ZEN group was lower than that in the positive control, it reached 5.23 times that of the control, indicating a continuous increase in intracellular ROS and confirming that 30 μg/mL ZEN induces oxidative stress, consistent with the oxidative stress parameters measured (GSH and SOD). The ROS levels in the POD and LC degradation product groups were slightly elevated compared to the control, with fluorescence intensities of 1.41 and 1.66 times that of the control, respectively. This increase may be attributed to the superoxidative processes during POD and LC treatment, potentially generating oxidative byproducts and free oxygen molecules. Nevertheless, the ROS levels in these groups were significantly lower than in the ZEN group ($P < 0.001$). The generation of intracellular ROS is closely linked to oxidative stress, and prolonged exposure to high ROS levels can damage cellular structures and functions, leading to cell death. This study indicates that POD and LC effectively degrade ZEN, significantly reducing its cytotoxicity, primarily due to the lower toxicity of the metabolites produced during degradation. Notably, the ZEN degradation products after POD and LC treatment may also participate in other metabolic pathways, such as modulating the intracellular antioxidant enzyme system, thereby enhancing cellular defenses against oxidative stress.

3.6 Apoptosis and MMP

To determine the potential of ZEN, ZEN-POD and ZEN-LC enzymatic degradation products to induce apoptosis in HepaRG cells, we employed the Annexin V-FITC/PI double staining method for cellular labeling. The flow cytometry analysis presented in Fig. 6A depicted a two-dimensional dot plot, where viable cells negative for both Annexin V-FITC and PI staining were located in the lower left quadrant (Q4). Early apoptotic cells positive for Annexin V-FITC but negative for PI were found in the lower right quadrant (Q2), while necrotic cells negative for Annexin V-FITC but positive for PI were observed in the upper left quadrant (Q1). Late apoptotic/necroptotic cells positive for both Annexin V-FITC and PI were situated in the upper right quadrant (Q3). Our results revealed that following exposure to ZEN, HepaRG cells exhibited percentages of viable, necrotic, early apoptotic, and late apoptotic cells as (24.7 ± 1.3)%, (0.6 ± 0.1)%, (20.6 ± 0.2)%, and (54.0 ± 1.2)%, respectively, resulting in an overall apoptosis rate of (74.6 ± 1.3)% (Fig. 6C). These findings suggest that ZEN at a concentration of 30 μg/mL can significantly induce apoptosis ($P < 0.005$) within HepaRG cells. In contrast, when treated with ZEN-POD or ZEN-LC degradation products groups, the proportion of viable cells was determined to be approximately (94.2 ± 0.7)% and (94.1 ± 0.2)%, respectively, with total apoptosis rates within HepaRG cells being merely (5.6 ± 0.7)% and (5.7 ± 0.3)%. This indicates that compared to untreated control group, the degradation products generated by POD and LC did not significantly induce apoptosis within HepaRG cells.

Mitochondrial oxidative phosphorylation is a major source of endogenous oxidants. Recent studies have shown that excessive ROS can disrupt the MMP by activating the opening of the mitochondrial MPTP, thereby triggering the Caspase-dependent apoptosis pathway[35]. To objectively evaluate the impact of ZEN and its degradation products on MMP in HepaRG cells, we conducted JC-1 staining followed by flow cytometric analysis of MMP levels, as depicted in Fig. 6B. The red to green fluorescence intensity ratio

was 3.44 for the control group. Upon exposure to 30 μg/mL ZEN, there was a significant increase in green fluorescence accompanied by a decrease in red fluorescence ($P < 0.001$), resulting in a ratio reduction to 1.40, indicating that ZEN decreased MMP in HepaRG cells (Fig. 6D). At the same time, the apoptosis rate reached 74.6% (Fig. 6C), indicating that mitochondrial pathway apoptosis is the core mechanism of ZEN-induced hepatotoxicity. The sustained opening of the MPTP leads to mitochondrial matrix swelling, outer membrane rupture, and cytochrome C release, ultimately activating the downstream apoptotic execution molecule Caspase-3[36]. In comparison with the control group, no significant differences were observed for MMP levels between the ZEN-LC degradation products group (3.11) and controls, while significantly lower MMP levels were detected for the ZEN-POD degradation products group (2.72) compared to controls ($P < 0.01$). However, both POD and LC degradation products groups exhibited significantly higher MMP levels than those treated with ZEN alone ($P < 0.001$). These findings suggest that the effects of ZEN degradation products on MMP are considerably less pronounced than those exerted by ZEN itself.

3.7 Metabolic profiling analysis

High-resolution mass spectrometry scan data of cell samples were processed for deconvolution and peak alignment using Compound Discover 3.1 software. Metabolite identification was performed via databases including mzCloud, ChemSpider, and MassBank. Subsequently, metabolites were screened based on fold change (FC), variable importance in projection (VIP), and statistical

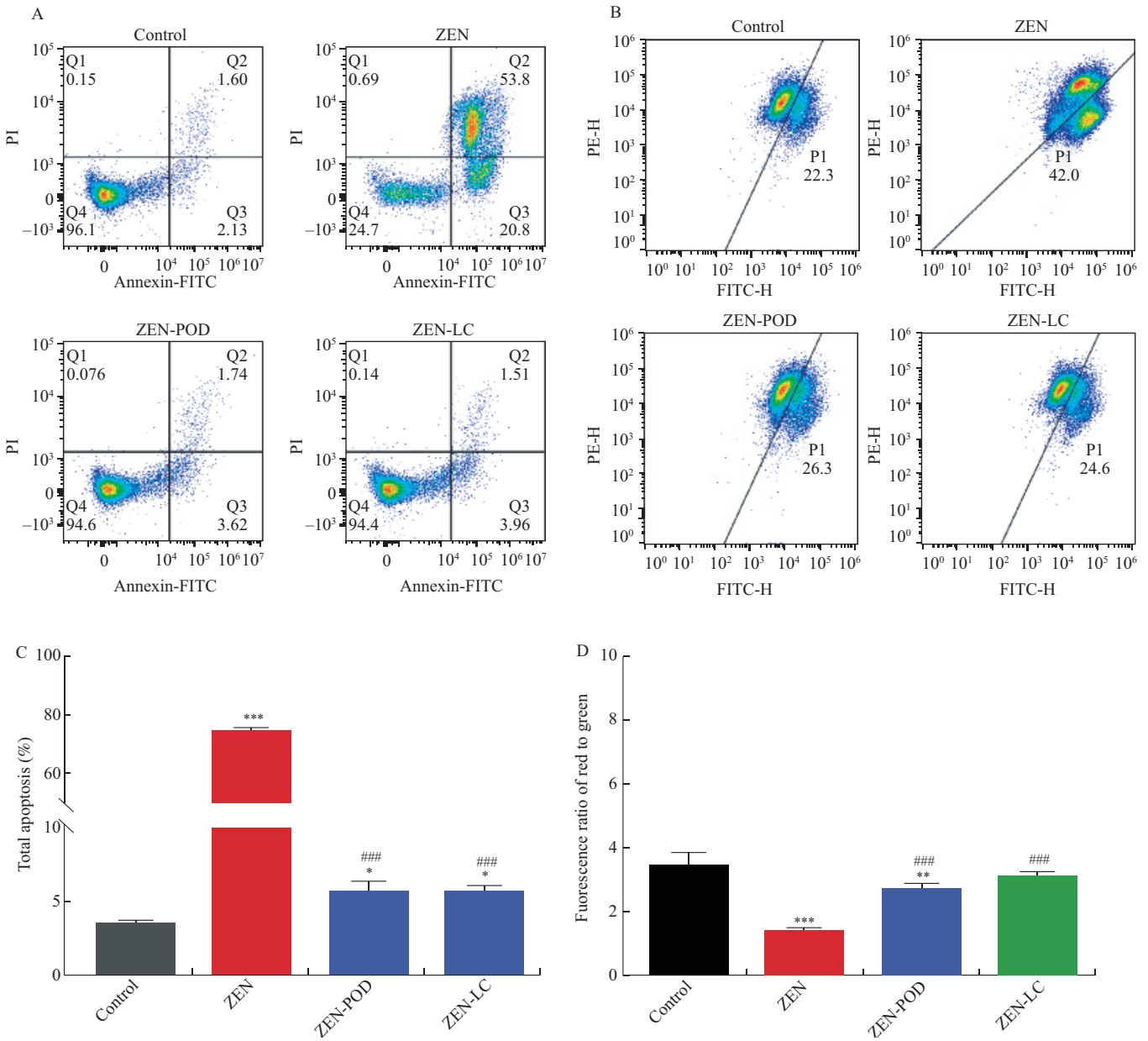


Fig. 6 Detoxification effects of POD and LC mediated ZEN degradation on HepaRG cells ($n = 6$). (A) Apoptosis of HepaRG cells was evaluated after exposure to ZEN, ZEN-POD and ZEN-LC enzymatic degradation products. (B) MMP of HepaRG cells was evaluated after exposure to ZEN, ZEN-POD and ZEN-LC enzymatic degradation products. (C) Statistical analysis of apoptosis. (D) Statistical analysis of MMP.

significance (*P*-values). Differential metabolites were selected from the ZEN group, ZEN-POD degradation product group, and ZEN-LC degradation product group employing criteria of VIP > 1, FC > 2 or < 0.5, and *t*-test $P < 0.05$ to investigate the impact of ZEN, POD, and LC degradation products on small molecule metabolism in HepaRG cells. Metabolite expression was visualized using a volcano plot depicted in Fig. 7A with $\log_2$ FC represented on the *y*-axis and –lg *P* represented on the *y*-axis. Each point represents a metabolite with colors indicating differential expression of compounds. Metabolites below the $P = 0.05$ line on the *y*-axis are considered unchanged relative to the control group ($P > 0.05$), while those above indicate significant differences ($P < 0.05$). Upregulated metabolites compared to control are denoted by red points whereas downregulated metabolites are denoted by green points. The counts of differential metabolites in the ZEN group, ZEN-POD degradation product group, and ZEN-LC degradation product group were 234, 76, and 65 respectively. In HepaRG cells treated with ZEN alone there were 156 downregulated metabolites and 78 upregulated ones; while treatment with POD led to downregulation of 62 metabolites along with upregulation of 14. Similarly, treatment with LC resulted in downregulation of 47 metabolites accompanied by upregulation of 18. The reduction in differential metabolites observed in cells treated with POD and LC after exposure to ZEN suggests that enzymatic products have a comparatively lesser impact on cellular metabolism compared to native ZEN, thereby partially demonstrating the detoxification effect of enzymatic treatment on ZEN[37-38].

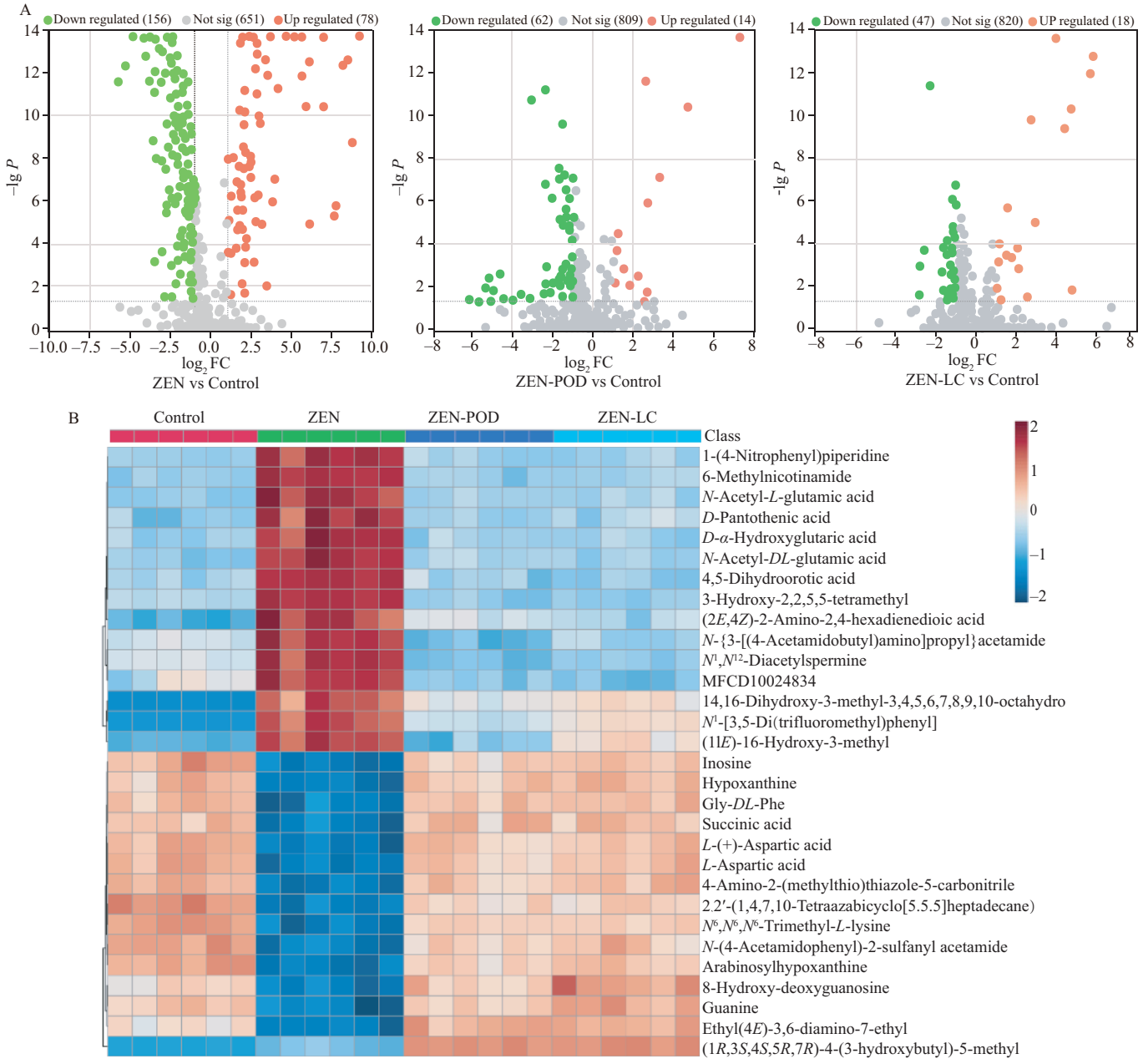


Fig. 7 Effects of enzymatic degradation of ZEN on the metabolism of HepaRG cells ($n = 6$). (A) Volcano plot of differential metabolites in HepaRG cells treated with ZEN, ZEN-POD and ZEN-LC enzymatic degradation products. (B) Clustered heatmap of the top 30 altered metabolites in HepaRG cells following exposure to ZEN and enzymatic degradation products of ZEN.

The differential metabolite data were imported into the Metaboanalyst website, where they underwent log transformation and Pareto normalization before being visually analyzed using a clustering heatmap. Based on *P*-values and hierarchical Pearson clustering (Fig. 7B), the top 30 differential metabolites of the control group, ZEN group, ZEN-POD degradation product group, and ZEN-LC degradation product group were displayed. The results indicate that amino acids, nucleotides and vitamins are the primary types of metabolites influenced by ZEN. Similar metabolic patterns were observed among the control group, ZEN-POD degradation product group, and ZEN-LC degradation product group with consistent concentration changes in most of the top 30 differential metabolites; however, significant differences were found between the ZEN group and control group. This result further demonstrates that enzymatic treatment of ZEN with POD and LC reduces its toxicity to liver cells.

3.8 Metabolic pathway analysis

The Metaboanalyst 6.0 platform was utilized for comprehensive analysis of key metabolic pathways in cells treated with ZEN, ZEN-POD, and ZEN-LC. Enrichment and topological analyses were conducted, and the results were visualized using the Bioinformatics tool. The horizontal axis represents pathway impact values derived from topological analysis, while the vertical axis displays the negative logarithm of *P*-values calculated during enrichment analysis. Circle sizes on the plot correspond to the number of key metabolites affected within each pathway. In HepaRG cells exposed to ZEN, significant alterations were observed in 5 major metabolic pathways: amino acid metabolism, carbohydrate metabolism, lipid metabolism, cofactor and vitamin metabolism, as well as nucleotide metabolism. Among these pathways, a total of 49 key differential metabolites were regulated, with 40 metabolites being reversed in the ZEN-POD degradation products group and 38 in the ZEN-LC degradation products group.

ZEN significantly modulated the metabolism of HepaRG cells across eight amino acid pathways, including taurine and hypotaurine metabolism; alanine, aspartate, and glutamate metabolism; cysteine and methionine metabolism; glycine, serine, and threonine metabolism; arginine and proline metabolism; arginine biosynthesis; tyrosine metabolism; and glutathione metabolism (Fig. 8A). A total of 19 compounds related to amino acid metabolism were regulated, including upregulation of *N*-acetylputrescine, *N*-acetyl-*L*-glutamate, *N*-acetyl-*L*-aspartate, *L*-proline, *L*-aspartate, high vanillate and *L*-adrenaline, and downregulation of succinate, *N*-(*L*-arginine) succinate, *L*-serine, *L*-cysteine, *L*-cystathionine, *L*-alanine, hypotaurine, glycocholic acid, creatine, choline, 3-phosphoglycerate, and citrate. Researches have demonstrated that ZEN can inhibit the expression of multiple amino acids in serum and protein synthesis[39-40]. In the ZEN-POD and ZEN-LC degradation products groups, reduction in 15 and 14 compounds related to amino acid metabolism was observed, respectively, enrichment being seen only in 3 and 4 pathways (Figs. 8B, C). This suggests that the impact of ZEN on amino acid metabolism is diminished following POD and LC degradation. Furthermore, succinate and citrate were downregulated in the presence of ZEN group indicating a

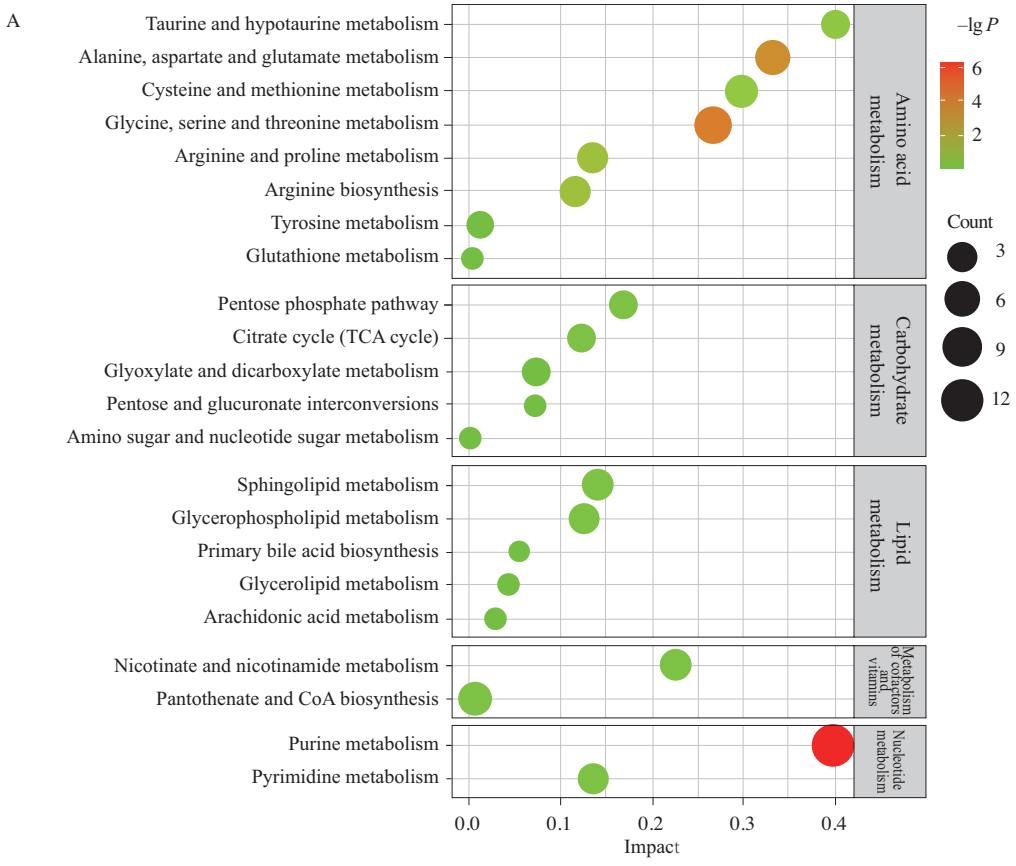


Fig. 8 Topological map of the metabolic pathways in HepaRG cells influenced by ZEN, ZEN-POD and ZEN-LC enzymatic degradation products. A-C respectively denote the impacts of ZEN, ZEN-POD and ZEN-LC enzymatic degradation products on cellular metabolic pathways.

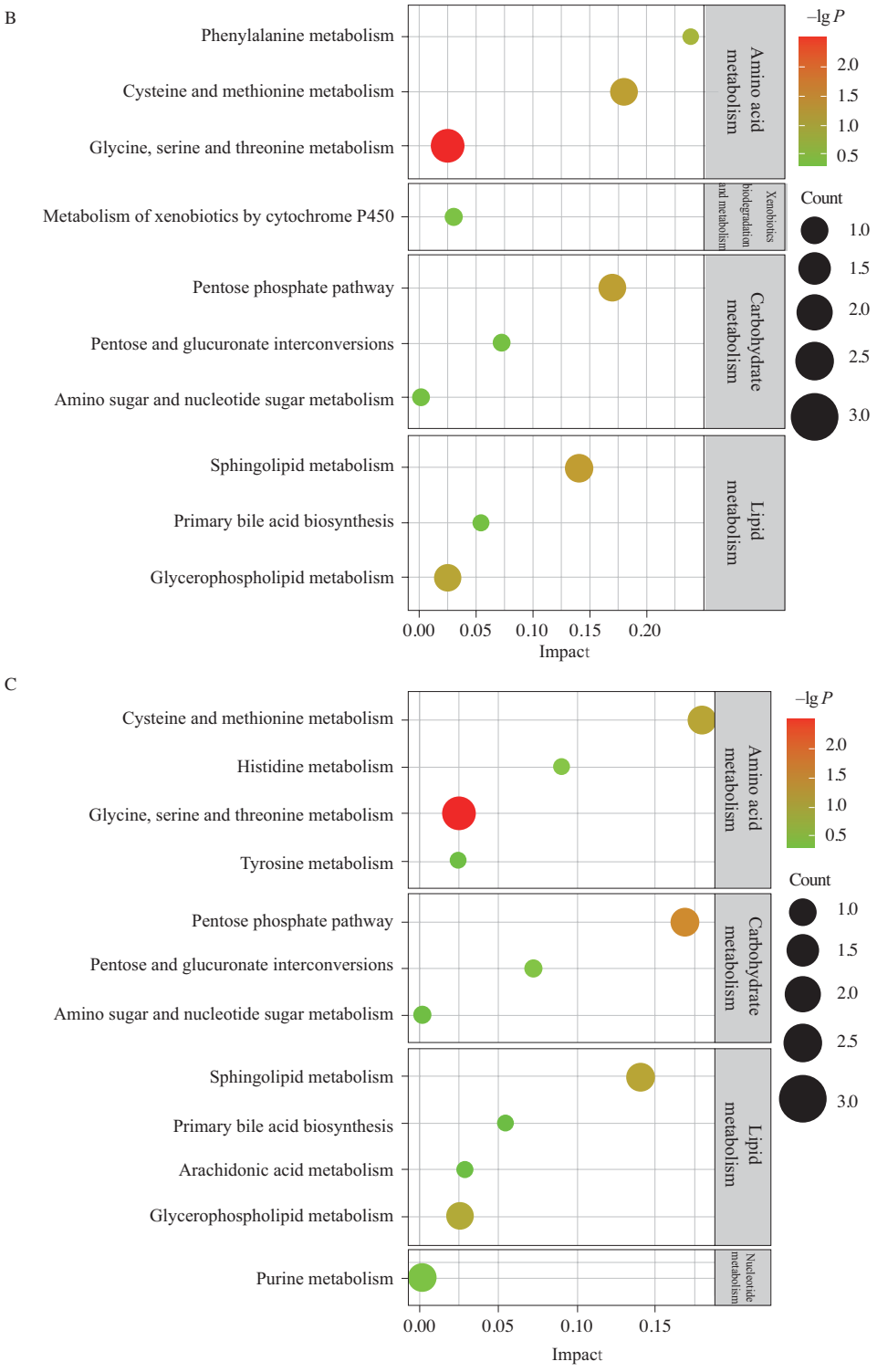


Fig. 8 (*Continued*)

significant inhibitory effect on tricarboxylic acid cycle (TCA) which is crucial for ZEN-induced cytotoxicity[41]. However, this inhibitory effect was completely absent in the ZEN-POD and ZEN-LC groups. Combining the observed changes in amino acid and energy metabolism pathways suggests that the degradation of ZEN by POD and LC primarily mitigates its toxicity through these pathways.

Lipid metabolism plays a pivotal role in various essential signal transduction processes, encompassing cell growth, differentiation, aging, and programmed cell death, and is implicated in diverse metabolic disorders[42]. This study identified significant perturbations in sphingolipid metabolism, glycerophospholipid metabolism, primary bile acid biosynthesis, glycerolipid metabolism, and arachidonic acid metabolism within the ZEN group, aligning with previous findings on ZEN's impact on lipid metabolism in porcine intestinal epithelial IPEC-J2 cells[43]. Within the ZEN group, there was an elevation observed in sphingosine and *sn*-3 phosphatidylglycerol

levels alongside a reduction in sphingomyelin content as well as *L*-serine and other related metabolites. In contrast to this observation within the ZEN group alone, however, the alterations seen in *sn*-3 phosphatidylglycerol and *L*-serine levels were reversed upon treatment with POD or LC degradation products of ZEN. This suggests that POD and LC degradation products mediate detoxification of ZEN through modulation of lipid metabolism. Furthermore, the reversal of cofactor and vitamin metabolic pathways along with nucleotide metabolism was evident specifically within the ZEN-POD group while cofactor and vitamin metabolic pathways were reversed within the ZEN-LC group. Notably, research has identified that POD degradation products generate novel metabolites as well as metabolic pathways within liver cells. Chloroacetyl chloride accumulation during cytochrome P450-mediated xenobiotic metabolism was not observed in the ZEN and ZEN-LC groups. In most organisms, cytochrome P450 monooxygenase, the primary phase I enzyme involved in xenobiotic detoxification, tends to convert lipophilic toxins into hydrophilic metabolites[44].

4. Conclusion

This study demonstrates that commercial POD and LC effectively alleviate ZEN-induced hepatotoxicity through catalytic degradation, with POD uniquely cleaving ZEN's lactone ring-a novel detoxification mechanism. Enzymatic treatment restored 90% cell viability, normalized oxidative/apoptotic markers, and rebalanced metabolic pathways, providing a scalable food/feed detoxification strategy that warrants validation in real-world matrices to address potential synergies of degradation products and long-term biosafety.

Declaration of competing interest

Yongning Wu is an editorial board member for *Food Science and Human Wellness* and was not involved in the editorial review or the decision to publish this article. All authors declare that there are no competing interests.

Acknowledgements

This work was financially supported by the National Key Research and Development Program of China (2022YFF1102500) and the Key Research and Development Projects in Hubei Province, China (2021BCA113).

Appendix A. Supplementary data

Supplementary data associated with this article can be found, in the online version, at http://doi.org/10.26599/FSHW.2025.9250539.

References

[1] B. Murtaza, X. Li, L. Dong, et al., Microbial and enzymatic battle with food contaminant zearalenone (ZEN), Appl. Microbiol. Biotechnol. 106 (2022) 4353-4365. https://doi.org/10.1007/s00253-022-12009-7.

[2] M.E. Flores-Flores, E. Lizarraga, A.L. De Cerain, et al., Presence of mycotoxins in animal milk: a review, Food Control 53 (2015) 163-176. https://doi.org/10.1016/j.foodcont.2015.01.020.

[3] EFSA Panel on Contaminants in the Food Chain (CONTAM), Scientific opinion on the risks for public health related to the presence of zearalenone in food, EFSA Journal 9 (2011) 2197. https://doi.org/10.2903/j.efsa.2011.2197.

[4] J. Chen, The Chinese experience in total diet studies, in: G.G. Moy, R.W. Vannoort (Eds.), Total Diet Studies, Springer New York, New York, NY, 2013: pp. 245-252. https://doi.org/10.1007/978-1-4419-7689-5_23.

[5] D.K. Mahato, S. Devi, S. Pandhi, et al., Occurrence, impact on agriculture, human health, and management strategies of zearalenone in food and feed: a review, Toxins 13 (2021) 92. https://doi.org/10.3390/toxins13020092.

[6] X. Bai, C. Sun, J. Xu, et al., Detoxification of zearalenone from corn oil by adsorption of functionalized GO systems, Applied Surface Science 430 (2018) 198-207. https://doi.org/10.1016/j.apsusc.2017.06.055.

[7] M. Liu, L. Zhao, G. Gong, et al., Invited review: remediation strategies for mycotoxin control in feed, J. Animal. Sci. Biotechnol. 13 (2022) 19. https://doi.org/10.1186/s40104-021-00661-4.

[8] I. Vanhoutte, K. Audenaert, L. De Gelder, Biodegradation of mycotoxins: tales from known and unexplored worlds, Front. Microbiol. 7 (2016) 561. https://doi.org/10.3389/fmicb.2016.00561.

[9] K.V. Marimón Sibaja, S. De Oliveira Garcia, A.C.P. Feltrin, et al., Aflatoxin biotransformation by commercial peroxidase and its application in contaminated food, J. Chemical Tech. Biotech. 94 (2019) 1187-1194. https://doi.org/10.1002/jctb.5865.

[10] A.C. Penteado Feltrin, M. Ramos Vaz Fontes, H. Delgado Kikumoto Gracia, et al., Peroxidase from soybean meal: obtention, purification and application in reduction of deoxynivalenol levels, Quim. Nova 40(8) (2017) 908-915. https://doi.org/10.21577/0100-4042.20170088.

[11] X. Qin, X. Su, T. Tu, et al., Enzymatic degradation of multiple major mycotoxins by dye-decolorizing peroxidase from Bacillus subtilis, Toxins 13 (2021) 429. https://doi.org/10.3390/toxins13060429.

[12] F.D. Ayodeji, B. Shava, H.M.N. Iqbal, et al., Biocatalytic versatilities and biotechnological prospects of laccase for a sustainable industry, Catal. Lett. 153 (2023) 1932-1956. https://doi.org/10.1007/s10562-022-04134-9.

[13] A. Mayer, Laccase: new functions for an old enzyme, Phytochemistry 60 (2002) 551-565. https://doi.org/10.1016/S0031-9422(02)00171-1.

[14] F. Sun, D. Yu, H. Zhou, et al., CotA laccase from *Bacillus licheniformis* ZOM-1 effectively degrades zearalenone, aflatoxin B_1 and alternariol, Food Contr. 145 (2023) 109472. https://doi.org/10.1016/j.foodcont.2022.109472.

[15] X. Wang, Y. Bai, H. Huang, et al., Degradation of aflatoxin B_1 and zearalenone by bacterial and fungal laccases in presence of structurally defined chemicals and complex natural mediators, Toxins 11 (2019) 609. https://doi.org/10.3390/toxins11100609.

[16] Z. Zhou, R. Li, T.B. Ng, et al., A new laccase of Lac 2 from the white rot fungus Cerrena unicolor 6884 and Lac 2-mediated degradation of aflatoxin B_1, Toxins 12 (2020) 476. https://doi.org/10.3390/toxins12080476.

[17] M. Liu, X. Zhang, H. Luan, et al., Bioenzymatic detoxification of mycotoxins, Front. Microbiol. 15 (2024) 1434987. https://doi.org/10.3389/fmicb.2024.1434987.

[18] S.O. Garcia, A.C.P. Feltrin, J. Garda-Buffon, Zearalenone reduction by commercial peroxidase enzyme and peroxidases from soybean bran and rice bran, Food Additives & Contaminants: Part A 35 (2018) 1819-1831. https://doi.org/10.1080/19440049.2018.1486044.

[19] X. Qin, Y. Xin, J. Zou, et al., Efficient degradation of aflatoxin B_1 and zearalenone by laccase-like multicopper oxidase from Streptomyces thermocarboxydus in the Presence of Mediators, Toxins 13 (2021) 754. https://doi.org/10.3390/toxins13110754.

[20] X. Wan, W. Jia, Q. Wang, et al., Metabolomics strategy comprehensively unveils the effect of catechins intervention on the biomarkers of exposure to acrylamide and biomarkers of cardiometabolic risk, Environ. Int. 169 (2022) 107517. https://doi.org/10.1016/j.envint.2022.107517.

[21] X. Zhang, X. Dai, X. Zhao, et al., MiR-874-3p represses the migration and invasion yet promotes the apoptosis and cisplatin sensitivity via being sponged by long intergenic non-coding RNA 00922 (LINC00922) and targeting glycerophosphodiester phosphodiesterase domain containing 5 (GDPD5) in gastric cancer cells, Bioengineered 13 (2022) 7082-7104. https://doi.org/10.1080/21655979.2022.2045831.

[22] N. Mansouri, O. Benslama, R. Arhab, Homology modeling, docking and molecular dynamics studies of some secondary metabolites of actinomycetes as biocontrol agents against the 3HNR enzyme of the phytopathogenic fungus *Alternaria alternata*, J. Biomolecular Structure and Dynamics 41 (2023) 871-883. https://doi.org/10.1080/07391102.2021.2014970.

[23] Y. Guo, Y. Wang, Y. Tang, et al., Combined *in silico* investigation and in vitro characterization of the zearalenone detoxification potential of dye-decolorizing peroxidase from *Bacillus subtilis* 168, Food Contr. 146 (2023) 109549. https://doi.org/10.1016/j.foodcont.2022.109549.

[24] Y.Z. Weng, D.T.H. Chang, Y.F. Huang, et al., A study on the flexibility of enzyme active sites, BMC Bioinf. 12 (2011) S32. https://doi.org/10.1186/1471-2105-12-S1-S32.

[25] L.I. Matienko, E.M. Mil, A.A. Albantova, et al., The role H-bonding and supramolecular structures in homogeneous and enzymatic catalysis, IJMS 24 (2023) 16874. https://doi.org/10.3390/ijms242316874.

[26] S. Ding, C. Lin, Q. Xiao, et al., Effective degradation of zearalenone by dye-decolorizing peroxidases from *Pleurotus ostreatus* and its metabolic pathway and toxicity analysis, Sci. Total Environ. 908 (2024) 168500. https://doi.org/10.1016/j.scitotenv.2023.168500.

[27] P. Li, R. Su, R. Yin, et al., Detoxification of mycotoxins through biotransformation, Toxins 12 (2020) 121. https://doi.org/10.3390/toxins12020121.

[28] D. Singh, N. Gupta, Microbial laccase: a robust enzyme and its industrial applications, Biologia 75 (2020) 1183-1193. https://doi.org/10.2478/s11756-019-00414-9.

[29] S. Damiano, C. Longobardi, E. Andretta, et al., Antioxidative effects of curcumin on the hepatotoxicity induced by ochratoxin A in rats, Antioxidants 10 (2021) 125. https://doi.org/10.3390/antiox10010125.

[30] R. Ferriero, E. Nusco, R. De Cegli, et al., Pyruvate dehydrogenase complex and lactate dehydrogenase are targets for therapy of acute liver failure, J. Hepatol. 69 (2018) 325-335. https://doi.org/10.1016/j.jhep.2018.03.016.

[31] X. He, S. Li, Y. Li, et al., Evaluation of reduced toxicity of zearalenone as measured by the HepG2 cell assay on degradation enzymes, Food Contr. 57 (2015) 161-168. https://doi.org/10.1016/j.foodcont.2015.03.031.

[32] Q. Huang, S. Ma, T. Tominaga, et al., An 8-week, low carbohydrate, high fat, ketogenic diet enhanced exhaustive exercise capacity in mice part 2: effect on fatigue recovery, post-exercise biomarkers and anti-oxidation capacity, Nutrients 10 (2018) 1339. https://doi.org/10.3390/nu10101339.

[33] J. Lu, Z. Wang, J. Cao, et al., A novel and compact review on the role of oxidative stress in female reproduction, Reprod. Biol. Endocrinol. 16 (2018) 80. https://doi.org/10.1186/s12958-018-0391-5.

[34] Y.Y. Wang, Y.C. Sun, X.F. Sun, et al., Starvation at birth impairs germ cell cyst breakdown and increases autophagy and apoptosis in mouse oocytes, Cell Death Dis. 8 (2017) e2613. https://doi.org/10.1038/cddis.2017.3.

[35] Q. Zhang, W. Chen, B. Zhang, et al., Central role of TRAP1 in the ameliorative effect of oleanolic acid on the mitochondrial-mediated and endoplasmic reticulum stress-excitated apoptosis induced by ochratoxin A, Toxicology 450 (2021) 152681. https://doi.org/10.1016/j.tox.2021.152681.

[36] Q. Wang, W. Chen, B. Zhang, et al., Perfluorooctanoic acid induces hepatocellular endoplasmic reticulum stress and mitochondrial-mediated apoptosis *in vitro* via endoplasmic reticulum-mitochondria communication, Chemico-Biological Interactions 354 (2022) 109844. https://doi.org/10.1016/j.cbi.2022.109844.

[37] Y. Fang, Z. Zhang, W. Xu, et al., Zearalenone lactonase: characteristics, modification, and application, Appl. Microbiol. Biotechnol. 106 (2022) 6877-6886. https://doi.org/10.1007/s00253-022-12205-5.

[38] J. Gari, R. Abdella, Degradation of zearalenone by microorganisms and enzymes, PeerJ 11 (2023) e15808. https://doi.org/10.7717/peerj.15808.

[39] E.K.K. Lo, X. Wang, P.K. Lee, et al., Mechanistic insights into zearalenone-accelerated colorectal cancer in mice using integrative multi-omics approaches, Comput. Struct. Biotechnol. J. 21 (2023) 1785-1796. https://doi.org/10.1016/j.csbj.2023.02.048.

[40] Z.O.B. Othmen, E.E. Golli, S. Abid-Essefi, et al., Cytotoxicity effects induced by zearalenone metabolites, α zearalenol and β zearalenol, on cultured Vero cells, Toxicology 252 (2008) 72-77. https://doi.org/10.1016/j.tox.2008.07.065.

[41] A. Gerdemann, M. Behrens, M. Esselen, et al., Metabolic profiling as a powerful tool for the analysis of cellular alterations caused by 20 mycotoxins in HepG2 cells, Arch Toxicol. 96 (2022) 2983-2998. https://doi.org/10.1007/s00204-022-03348-5.

[42] Q. Wang, Y. Li, P. Hu, et al., Impact of enniatins and beauvericin on lipid metabolism: insights from a 3D HepaRG spheroid model, Environ. Int. 191 (2024) 108969. https://doi.org/10.1016/j.envint.2024.108969.

[43] H. Wang, Y. Xiao, C. Xu, et al., Integrated metabolomics and transcriptomics analyses reveal metabolic mechanisms in porcine intestinal epithelial cells under zearalenone stress, J. Agric. Food Chem. 70 (2022) 6561-6572. https://doi.org/10.1021/acs.jafc.2c01107.

[44] M.R. Berenbaum, D.S. Bush, L.H. Liao, Cytochrome P450-mediated mycotoxin metabolism by plant-feeding insects, Curr. Opin. Insect Sci. 43 (2021) 85-91. https://doi.org/10.1016/j.cois.2020.11.007.